New Ambipolar Organic Semiconductors. 2. Effects of Electron Acceptor Strength on Intramolecular Charge Transfer Photophysics, Highly Efficient Electroluminescence, and Field-Effect Charge Transport of Phenoxazine-Based Donor−Acceptor Materials

Abhishek P. Kulkarni, Yan Zhu, Amit Babel, Pei-Tzu Wu, and Samson A. Jenekhe*

Departments of Chemical Engineering and Chemistry, University of Washington, Seattle, Washington 98195

Received August 7, 2007. Revised Manuscript Received March 29, 2008

Substantial variations (up to factors of 5) were observed in the intramolecular charge-transfer (ICT) fluorescence quantum yields and electroluminescence efficiencies among a series of emissive bipolar donor−acceptor (D−A) materials based on a phenoxazine donor and different acceptors with a varying electron acceptor strength, including quinoline, quinoxaline, benzoquinoxaline, and benzoylquinoxaline. High-efficiency organic light-emitting diodes (OLEDs) with colors spanning the visible spectrum were achieved from the new emissive ambipolar materials. The performance of the OLEDs based on the D−A molecules decreased with increasing electron acceptor strength, largely owing to the reduction in fluorescence efficiencies. Green OLEDs (CIE = 0.27, 0.61) from a phenoxazine-quinoline molecule gave the best performance (36190 cd/m^2, 10.9 cd/A at 5115 cd/m^2). Red OLEDs (CIE = 0.63, 0.37) with moderate performance (9580 cd/m^2, 2.3 cd/A at 230 cd/m^2) were obtained from the phenoxazine-benzoylquinoxaline molecule. These results show that the electron accepting strength of the acceptor moiety in a D−A molecule is a convenient method for varying the HOMO/LUMO energy levels and the resultant electroluminescence emission colors. Field-effect hole mobilities of up to 7×10^{-4} cm^2/Vs were obtained in the phenoxazine-quinoline D−A molecules, demonstrating the potential of phenoxazine as a building block for developing new emissive and charge-transport materials for OLEDs.

Introduction

Organic light-emitting diodes (OLEDs) are currently being developed for applications in full-color displays and solid-state lighting, with some consumer devices such as cell phones and digital cameras incorporating OLED screens already available in the market.[1–3] Donor−acceptor (D−A) small molecules are being explored as the active emissive elements in high-performance OLEDs because of their attractive properties such as bipolar charge (electron and hole) transport and high solid-state photoluminescence quantum yield.[4–12] The electroluminescence (EL) from such D−A molecules invariably originates from their intramolecular charge transfer (ICT) excited states;[11a] in some cases, emission from intermolecular excimers or exciplexes may arise.[11d,13,14] Thus, the HOMO/LUMO levels and the emission color of the D−A molecule can be simultaneously

* Corresponding author. E-mail: jenekhe@u.washington.edu.

(1) (a) Reviews on various aspects of organic electroluminescence: (a) Kraft, A.; Grimsdale, A. C.; Holmes, A. B. *Angew. Chem., Int. Ed.* **1998**, *37*, 402. (b) Mitschke, U.; Bauerle, P. J. *J. Mater. Chem.* **2000**, *10*, 1471. (c) Kulkarni, A. P.; Tonzola, C. J.; Babel, A.; Jenekhe, S. A. *Chem. Mater.* **2004**, *16*, 4556.

(2) (a) Yan, H.; Lee, P.; Armstrong, N. R.; Graham, A.; Evmenenko, G. A.; Dutta, P.; Marks, T. J. *J. Am. Chem. Soc.* **2005**, *127*, 3172. (b) Furuta, P. T.; Deng, L.; Garon, S.; Thompson, M. E.; Frechet, J. M. J. *J. Am. Chem. Soc.* **2004**, *126*, 15388. (c) Tarkka, R. M.; Zhang, X.; Jenekhe, S. A. *J. Am. Chem. Soc.* **1996**, *118*, 9438. (d) Kulkarni, A. P.; Jenekhe, S. A. *Macromolecules* **2003**, *36*, 5285. (e) Kulkarni, A. P.; Zhu, Y.; Jenekhe, S. A. *Macromolecules* **2005**, *38*, 1553.

(3) (a) Jenekhe, S. A.; Zhang, X.; Chen, X. L.; Choong, V.-E.; Gao, Y.; Hsieh, B. R. *Chem. Mater.* **1997**, *9*, 409. (b) Zhang, X.; Shetty, A. S.; Jenekhe, S. A. *Macromolecules* **1999**, *32*, 7422. (c) Zhang, X.; Jenekhe, S. A. *Macromolecules* **2000**, *33*, 2069. (d) Tonzola, C. J.; Alam, M. M.; Jenekhe, S. A. *Adv. Mater.* **2002**, *14*, 1086. (e) Zhang, X.; Kale, D. M.; Jenekhe, S. A. *Macromolecules* **2002**, *35*, 382. (f) Alam, M. M.; Tonzola, C. J.; Jenekhe, S. A. *Macromolecules* **2003**, *36*, 6577.

(4) (a) Hamada, Y.; Adachi, C.; Tsutsui, T.; Saito, S. *Jpn. J. Appl. Phys* **1992**, *31*, 1812. (b) Tamoto, N.; Adachi, C.; Nagai, K. *Chem. Mater.* **1997**, *9*, 1077. (c) Antoniadis, H.; Inbasekaran, M.; Woo, E. P. *Appl. Phys. Lett.* **1998**, *73*, 3055.

(5) (a) Shirota, Y.; Kinoshita, M.; Noda, T.; Okumoto, T.; Ohara, T. *J. Am. Chem. Soc.* **2000**, *122*, 11021. (b) Doi, H.; Kinoshita, M.; Okumoto, K.; Shirota, Y. *Chem. Mater.* **2003**, *15*, 1080. (c) Zhang, H.; Huo, C.; Zhang, J.; Zhang, P.; Tian, W.; Wang, Y. *Chem. Commun.* **2006**, 281.

(6) (a) Thomas, K. R. J.; Lin, J. T.; Tao, Y.-T.; Chuen, C.-H. *Chem. Mater.* **2002**, *14*, 3852. (b) Thomas, K. R. J.; Lin, J. T.; Tao, Y.-T.; Chuen, C.-H. *J. Mater. Chem.* **2002**, *12*, 3516. (c) Tao, Y.-T.; Chuen, C.-H.; Ko, C. W.; Peng, J. W. *Chem. Mater.* **2002**, *14*, 4256. (d) Thomas, K. R. J.; Lin, J. T.; Velusamy, M.; Tao, Y.-T.; Chuen, C.-H. *Adv. Funct. Mater.* **2004**, *14*, 83. (e) Chiang, C.-L.; Wu, M.-F.; Dai, D.-C.; Wen, Y.-S.; Wang, J.-K.; Chen, C.-T. *Adv. Funct. Mater.* **2005**, *15*, 231.

(7) Zhu, W.; Hu, M.; Yao, R.; Tian, H. *J. Photochem. Photobiol. A* **2003**, *154*, 169.

(8) Kelnhofer, K.; Knorr, A.; Tak, Y.-H.; Bassler, H.; Daub, J. *Acta Polym.* **1997**, *48*, 188.

(9) Goes, M.; Verhoeven, J. W.; Hofstraat, H.; Brunner, K. *ChemPhysChem* **2003**, *4*, 349.

(10) (a) Li, Z. H.; Wong, M. S.; Fukutani, H.; Tao, Y. *Org. Lett.* **2006**, *8*, 4271. (b) Chen, C.-T.; Wei, Y.; Lin, J.-S.; Moturu, M. V. R. K.; Chao, W.-S.; Tao, Y.-T.; Chien, C.-H. *J. Am. Chem. Soc.* **2006**, *128*, 10992. (c) Zhu, Y.; Gibbons, K. M.; Kulkarni, A. P.; Jenekhe, S. A. *Macromolecules* **2007**, *40*, 804.

(11) (a) Jenekhe, S. A.; Lu, L.; Alam, M. M. *Macromolecules* **2001**, *34*, 7315. (b) Kulkarni, A. P.; Wu, P.-T.; Kwon, T. W.; Jenekhe, S. A. *J. Phys. Chem. B* **2005**, *109*, 19584. (c) Zhu, Y.; Kulkarni, A. P.; Jenekhe, S. A. *Chem. Mater.* **2005**, *17*, 5225. (d) Kulkarni, A. P.; Kong, X.; Jenekhe, S. A. *Adv. Funct. Mater.* **2006**, *16*, 1057. (e) Hancock, J. M.; Gifford, A. P.; Zhu, Y.; Lou, Y.; Jenekhe, S. A. *Chem. Mater.* **2006**, *18*, 4924.

10.1021/cm7022136 CCC: $40.75
Published on Web 06/04/2008

manipulated through a choice of the D/A units. EL colors spanning the entire visible region have been obtained from D−A molecules of diverse architectures, including blue,[4a,6c,9,10a] green,[5,6a,7,10b,11,12c,d] yellow,[6a,b,8] and red.[6d,e,12a,b] In most of the current D−A molecules, the commonly used acceptor moieties include oxadiazole,[4,6a,12d] diarylboron,[5] quinoline,[11,12c,d] quinoxaline,[6b,10b] pyridopyrazine,[6b] and benzothiadiazole,[6d] whereas triarylamine,[4,5c,6c,d,11e,12a,d] carbazole,[6b,7,11a,d,12a] fluorene,[4c,10] and their combinations[5,6a,b] are the common donor blocks. There is a need for new D−A building blocks that are thermally and electrochemically robust to develop next generation emissive materials for OLEDs.

Although EL colors spanning the whole visible region have been demonstrated from many D−A molecules, they have generally been obtained from random combinations of different D and A moieties. Systematic approaches to tuning the EL colors by controlling the strength of ICT character via the electron donating or accepting moiety have been lacking. In the case of electron donating moieties, it is rather surprising that phenothiazine[11a–d,12a–c,15] and phenoxazine[11c,16] have been scarcely explored compared to carbazole and fluorene in current OLED materials, in spite of being stronger electron donors because of their ∼0.7 eV lower ionization potentials.[17] Both phenoxazine and phenothiazine have been extensively used in electron transfer reactions of donor/acceptor (D/A) molecular systems in solution in the context of electrogenerated chemiluminescence (ECL).[18,19] In addition, phenoxazine and phenothiazine are nonplanar fused ring systems with dihedral angles of ∼169 and 153°, respectively, relative to the planar carbazole and fluorene rings with a nearly 180° dihedral angle.[20] These differences in molecular geometry of the donor blocks should lead to significant differences in charge transport and emissive properties of the corresponding D−A molecules. These issues have not been studied in any detail yet, barring a few recent reports by our group on phenoxazine and phenothiazine-containing D−A small molecules for OLEDs[11a–d] and polymers for p-channel thin-film transistors (TFTs).[21a] We note that D−A molecules and polymers are being explored for applications in ambipolar TFTs since their inbuilt D−A architecture lends them amenable for ambipolar charge transport.[22,23] Very little is currently known about the mechanism of ambipolar charge transport in such D−A semiconductors and its dependence on molecular architecture, electron accepting/donating strength of D/A moieties, and the resultant ICT character.

In this paper, we report the effects of the electron acceptor strength on the photophysical and electroluminescent properties of a series of 8 D−A molecules incorporating phenoxazine as the donor and various acceptor moieties, including quinoline,[3,11,24] quinoxaline,[6b,10b,25] benzoquinoxaline, and benzoylquinoxaline. Field-effect charge transport in several of the D−A molecules was also measured. One of the main objectives of the work was to systematically tune the ICT emission colors by modulating the degree of ICT character using the electron acceptor strength as a tool. The molecular structures of all the phenoxazine molecules investigated, 3,7-bis-(biphenyl-4-yl)-10-hexyl-10*H*-phenoxazine (BP-HPO), 3,7-bis-(4-phenyl-quinolin-2-yl)-10-phenyl-10*H*-phenoxazine (PQ-PPO), 3,7-bis-(4-phenyl-quinolin-2-yl)-10-methyl-10*H*-phenoxazine (PQ-MPO), 3,7-bis-(4-methyl-quinolin-2-yl)-10-phenyl-10*H*-phenoxazine(MQ-PPO),3,7-bis-(4-methyl-quinolin-2-yl)-10-methyl-10*H*-phenoxazine (MQ-MPO), 3,7-bis-(3-phenyl-quinoxalin-2-yl)-10-phenyl-10*H*-phenoxazine (PQx-PPO), 3,7-bis-(3-phenyl-benzo[g]quinoxalin-2-yl)-10-phenyl-10*H*-phenoxazine (BQx-PPO), and {3-[7-(7-benzoyl-3-phenyl-quinoxalin-2-yl)-10-phenyl-10*H*-phenoxazin-3-yl]-2-phenyl-quinoxalin-6-yl}-phenyl-methanone (BzQx-PPO), are shown in Chart 1. The electron acceptor strength generally increases in that order among the series of molecules. The detailed synthesis, characterization, single-crystal structure analyses, electrochemical properties, and quantum-chemical calculations of the electronic structure of all the D−A molecules was reported separately

(12) (a) Sun, X.; Liu, Y.; Xu, X.; Yang, C.; Yu, G.; Chen, S.; Zhao, Z.; Qiu, W.; Li, Y.; Zhu, D. *J. Phys. Chem. B* **2005**, *109*, 10786. (b) Kim, Y.-H.; Kim, H.-S.; Lee, K.-H.; Kwon, S.-K.; Kim, S.-H. *Mol. Cryst. Liq. Cryst.* **2006**, *444*, 257. (c) Oh, J.-J.; Kim, K.-W.; Kim, M.-S.; Kwon, T.-W.; Park, D.-K.; Cho, S.-J.; Woo, H.-S. *Appl. Phys. Lett.* **2006**, *89*, 073504. (d) Xiang, N. J.; Lee, T. H.; Gong, M. L.; Tong, K. L.; So, S. K.; Leung, L. M. *Synth. Met.* **2006**, *156*, 270.

(13) (a) Förster, Th. *Angew. Chem., Int. Ed.* **1969**, *8*, 333. (b) Jenekhe, S. A.; Osaheni, J. A. *Science* **1994**, *265*, 765.

(14) (a) Osaheni, J. A.; Jenekhe, S. A. *Macromolecules* **1994**, *27*, 739. (b) *The Exciplex*; Gordon, M., Ware, W. R., Eds.; Academic Press: New York, 1975.

(15) (a) Kong, X.; Kulkarni, A. P.; Jenekhe, S. A. *Macromolecules* **2003**, *36*, 8992. (b) Hwang, D.-H.; Kim, S.-K.; Park, M.-J.; Lee, J.-H.; Koo, B.-W.; Kang, I.-N.; Kim, S.-H.; Zyung, T. *Chem. Mater.* **2004**, *16*, 1298. (c) Cho, N. S.; Park, J.-H.; Lee, S.-K.; Lee, J.; Shim, H.-K.; Park, M.-J.; Hwang, D.-H.; Jung, B.-J. *Macromolecules* **2006**, *39*, 177.

(16) (a) Okamoto, T.; Kozaki, M.; Doe, M.; Uchida, M.; Wang, G.; Okada, K. *Chem. Mater.* **2005**, *17*, 5504. (b) Ito, Y.; Shimada, T.; Ha, J.; Vacha, M.; Sato, H. *J. Polym. Sci., Part A: Polym. Chem.* **2006**, *44*, 4338. (c) Hwang, D.-H.; Lee, J.-D.; Lee, M.-J.; Lee, C. *Curr. Appl. Phys.* **2005**, *5*, 244.

(17) (a) Bloor, J. E.; Gilson, B. R.; Haas, R. J.; Zirkle, C. L. *J. Med. Chem.* **1970**, *13*, 922. (b) Bressler, D. C.; Fedorak, P. M.; Pickard, M. A. *Biotechnol. Lett.* **2000**, *22*, 1119.

(18) (a) Richter, M. M. *Chem. Rev.* **2004**, *104*, 3003. (b) Dini, D. *Chem. Mater.* **2005**, *17*, 1933.

(19) (a) Knorr, A.; Daub, J. *Angew. Chem., Int. Ed.* **1995**, *34*, 2664. (b) Slaterbeck, A. F.; Meehan, T. D.; Gross, E. M.; Wightman, R. M. *J. Phys. Chem. B* **2002**, *106*, 6088. (c) Lai, R. Y.; Fabrizio, E. F.; Lu, L.; Jenekhe, S. A.; Bard, A. J. *J. Am. Chem. Soc.* **2001**, *123*, 9112. (d) Lai, R. Y.; Kong, X.; Jenekhe, S. A.; Bard, A. J. *J. Am. Chem. Soc.* **2003**, *125*, 12631.

(20) (a) Kurahashi, M.; Fukuyo, M.; Shimada, A.; Furusaki, A.; Nitta, I. *Bull. Chem. Soc. Jpn.* **1969**, *42*, 2174. (b) Pan, D.; Phillips, D. L. *J. Phys. Chem. A* **1999**, *103*, 4737.

(21) (a) Zhu, Y.; Babel, A.; Jenekhe, S. A. *Macromolecules* **2005**, *38*, 7983. (b) Babel, A.; Jenekhe, S. A. *Macromolecules* **2003**, *36*, 7759.

(22) (a) Horowitz, G. *Adv. Mater.* **1998**, *10*, 365. (b) Dimitrakopoulos, C. D.; Malenfant, P. R. L. *Adv. Mater.* **2002**, *14*, 99. (c) Babel, A.; Jenekhe, S. A. *Adv. Mater.* **2002**, *14*, 371. (d) Babel, A.; Jenekhe, S. A. *J. Am. Chem. Soc.* **2003**, *125*, 13656. (e) Babel, A.; Wind, J. D.; Jenekhe, S. A. *Adv. Funct. Mater.* **2004**, *14*, 891.

(23) (a) Kunugi, Y.; Takimiya, K.; Negishi, N.; Otsubo, T.; Aso, Y. *J. Mater. Chem.* **2004**, *14*, 2840. (b) Yoon, M.-H.; DiBenedetto, S. A.; Facchetti, A.; Marks, T. J. *J. Am. Chem. Soc.* **2005**, *127*, 1348. (c) Yamamoto, T.; Yasuda, T.; Sakai, Y.; Aramaki, S. *Macromol. Rapid Commun.* **2005**, *26*, 1214. (d) Champion, R. D.; Cheng, K.-F.; Pai, C.-L.; Chen, W.-C.; Jenekhe, S. A. *Macromol. Rapid Commun.* **2005**, *26*, 1835.

(24) (a) Kulkarni, A. P.; Gifford, A. P.; Tonzola, C. J.; Jenekhe, S. A. *Appl. Phys. Lett.* **2005**, *86*, 061106. (b) Kwon, T. W.; Alam, M. M.; Jenekhe, S. A. *Chem. Mater.* **2004**, *16*, 4657. (c) Shetty, A. S.; Liu, E. B.; Lachicotte, R. J.; Jenekhe, S. A. *Chem. Mater.* **1999**, *11*, 2292.

(25) (a) Cui, Y.; Zhang, X.; Jenekhe, S. A. *Macromolecules* **1999**, *32*, 3824. (b) Yamamoto, T.; Sugiyama, K.; Kushida, T.; Inoue, T.; Kanbara, T. *J. Am. Chem. Soc.* **1996**, *118*, 3930. (c) O'Brien, D.; Weaver, M. S.; Lidzey, D. G.; Bradley, D. D. C. *Appl. Phys. Lett.* **1996**, *69*, 881.

Chart 1

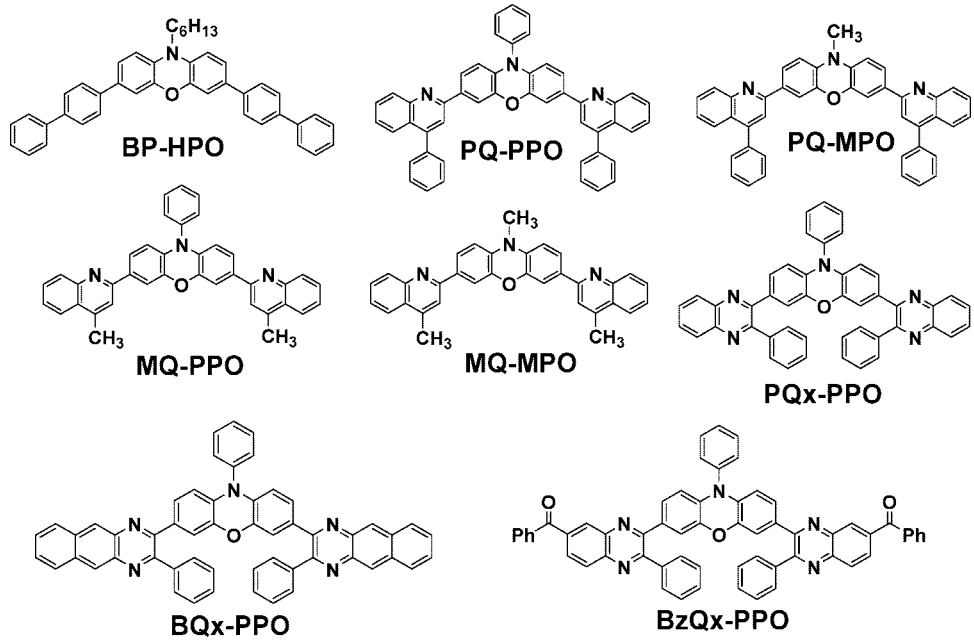

as part 1 in the series.[26] Herein we show that the ICT emission color of the D−A molecule can be varied from blue to green to yellow to red with increasing strength of the electron accepting moiety, not only in photoluminescence but also in solid-state electroluminescent devices. Simple OLEDs made from the emissive D−A molecules and tested in air had high brightness and high efficiencies because of their ambipolar redox properties and high fluorescence efficiencies. The electroluminescence of PQ-MPO and PQ-PPO was partly reported in a preliminary communication.[11c]

Experimental Section

Materials. The synthesis and structural characterization of the series of 8 donor−acceptor materials are reported separately elsewhere.[26]

Photophysical Characterization. UV−vis absorption spectra were recorded on a Perkin-Elmer model Lambda 900 UV/vis/near-IR spectrophotometer. The steady-state photoluminescence (PL) emission spectra were obtained with a Photon Technology International (PTI) Inc. model QM-2001−4 spectrofluorimeter. The PL quantum yields of the D−A molecules in toluene solution were measured by using a 1×10^{-5} M solution of perylene in toluene as a standard ($\phi_{PL} = 94\%$).[27] All solutions were degassed with nitrogen for 15−20 min before spectral acquisition.

Time-Resolved Photoluminescence Decay Dynamics. Fluorescence decays were measured on a PTI Model QM-2001−4 spectrofluorimeter equipped with Strobe Lifetime upgrade. The instrument utilizes a nanosecond flash lamp as an excitation source and a stroboscopic detection system. All measurements were done at room temperature. The decay curves were analyzed using a multiexponential fitting software provided by the manufacturer. Reduced χ^2 values, Durbin−Watson parameters, and weighted residuals were used as the goodness-of-fit criteria.

Fabrication and Characterization of OLEDs. Indium tin oxide (ITO)-coated glass substrates (Delta Technologies Ltd., Stillwater, MN) were cleaned sequentially in ultrasonic bathes of phosphate-free detergent, water, isopropanol, water, and acetone, and then dried at 60 °C in a vacuum oven overnight. A 60 nm thick poly(ethylenedioxythiophene)/poly(styrene sulfonate) blend (PEDOT; $\Phi = 5.2$ eV) hole-injection layer was spin-coated on top of ITO from a ∼0.75 wt % dispersion in water and dried at 200 °C for 15 min under a vacuum. Before spin-coating, the as-received PEDOT solution was diluted ∼25% with 1:1 (v/v) water:isopropanol and then filtered through 0.45 μm poly(vinylidenefluoride) (PVDF) syringe filters. A 10 nm thick hole-transport/electron-blocking layer of poly-*N*-vinylcarbazole (PVK) was obtained by spin-coating it on top of PEDOT from a 0.25 wt % solution in toluene and drying in a vacuum at 60 °C overnight. Before spin-coating, the PVK solutions were filtered through 0.2 μm poly(tetrafluoroethylene) (PTFE) syringe filters. The film thickness was measured by an Alpha-Step 500 surface profiler (KLA Tencor, Mountain View, CA). Thin films (35 nm thick) of each D−A molecule were deposited on top of the PVK film by evaporation from resistively heated quartz crucibles at a rate of ∼0.2 nm/s in a vacuum evaporator (Edwards Auto 306) at base pressures of $< 8 \times 10^{-7}$ Torr. A 30 nm thick hole-blocking layer of TPBI was then deposited on the D−A film without breaking the vacuum. The chamber was vented with air to load the cathode materials and pumped back down; a 2 nm LiF and a 110 nm thick aluminum layer were then sequentially deposited through a shadow mask on top of the TPBI film without breaking vacuum to form active diode areas of 0.2 cm^2. The resulting architecture of the diodes was ITO/PEDOT/PVK/D-A molecule/TPBI/LiF/Al.

(26) Zhu, Y.; Kulkarni, A. P.; Wu, P.-T.; Jenekhe, S. A. *Chem. Mater.* **2008**, *20*, 4200–4211.
(27) Heinrich, G.; Schoof, S.; Gusten, H. *J. Photochem.* **1974**, *3*, 315.

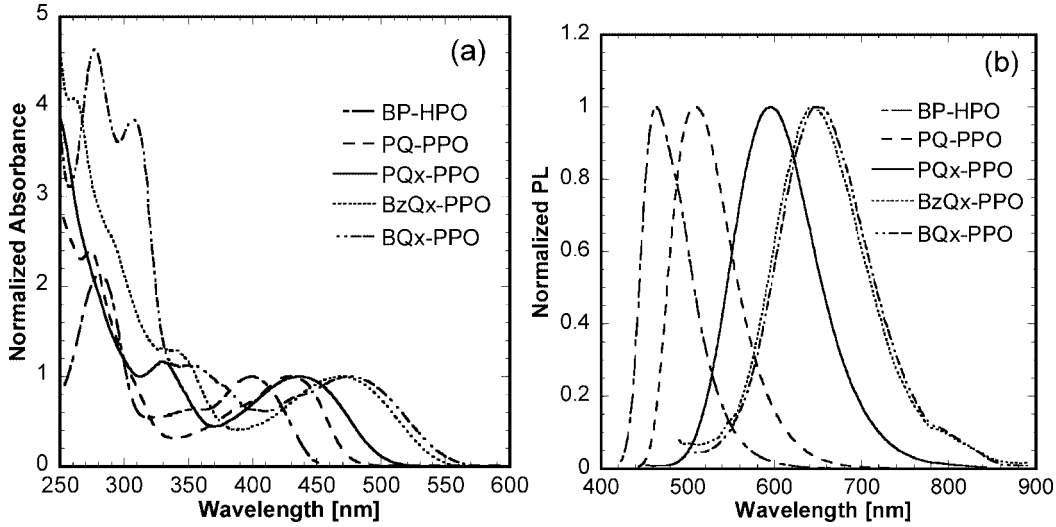

Figure 1. (a) Normalized optical absorption spectra and (b) PL emission spectra of five donor−acceptor molecules in dilute (2×10^{-5} M) 1,2-dichloroethane solution.

Electroluminescence spectra were obtained using a PTI QM-2001−4 spectrophotometer. Current−voltage characteristics of the LEDs were measured using a HP4155A semiconductor parameter analyzer (Yokogawa Hewlett-Packard, Tokyo). The luminance was simultaneously measured using a model 370 optometer (UDT instruments, Baltimore, MD) equipped with a calibrated luminance sensor head (model 211) and a 5× objective lens. The device external quantum efficiencies were calculated using procedures reported previously.[2d,11b–e] All the device fabrication and characterization steps were done under ambient laboratory air.

Fabrication and Characterization of Thin-Film Transistors. Field-effect transistors were fabricated from the four phenoxazine-quinoline D−A molecules by using the bottom contact geometry. Heavily doped Si with a conductivity of 10^3 S/cm was used as the gate electrode with a 300 nm thick SiO_2 layer as the gate insulator. By means of standard photolithography and a vacuum sputtering system (2×10^{-6} torr), two 90-nm thick gold electrodes (source and drain) with a 10 nm thick TiW alloy adhesive layer were fabricated onto the SiO_2/Si substrate. The FETs had a channel length (L) of 25 μm and channel width (W) of 500 μm. To complete the device, 30−40 nm thin films of each D−A molecule were deposited by vacuum evaporation. The substrate temperature was kept at room temperature. Electrical characteristics of these FETs were measured using a Keithley 4200 semiconductor parameter analyzer. All the fabrication and measurements were done under ambient laboratory air.

Results and Discussion

Photophysical Properties. (a) Solutions. Figure 1a shows the normalized optical absorption spectra of five D−A molecules in dilute (2×10^{-5} M) dichloroethane solution. Two prominent absorption features were observed in the spectra of all the D−A molecules: a lowest-energy band in the 400−480 nm range and high-energy bands in the 260−320 nm. In each D−A molecule, the high-energy peaks have larger extinction coefficients (ε) compared to that of the lowest-energy peak. The high-energy absorption bands are associated with the $\pi-\pi^*$ transitions of the D−A molecules, localized either on the D or A moiety of the molecule. The lowest-energy absorption band observed in all the molecules is completely absent in the absorption spectra of the parent D and A building blocks. This lowest-energy band can thus be assigned to the intramolecular charge transfer (ICT) transition $^1CT \leftarrow S_0$ in each D−A molecule.[11a,28] As the strength of the electron acceptor increases, the ICT absorption band of the D−A molecule red-shifts. For example, the ICT absorption maximum red-shifts from 429 nm in PQ-PPO to 438 nm in PQx-PPO to 478 nm in BQx-PPO with increasing electron acceptor strength from quinoline to quinoxaline to benzoquinoxaline. Given that the electron-donor moiety in all the molecules is the same, the observed red-shift can be understood to arise from the stronger ICT with increasing electron acceptor strength.

The absorption onset correspondingly red-shifts from ~475 nm in PQ-PPO to ~500 nm in PQx-PPO to ~540 nm in BQx-PPO, indicating a reduction in the optical band gap of the D−A molecule with increasing electron-accepting strength. The absorption onsets and peak maxima of BzQx-PPO and BQx-PPO are very similar, suggesting comparable ground-state ICT character, likely because of the similar electron accepting strength of the benzoylquinoxaline and benzoquinoxaline moieties. As expected, the four molecules containing quinoline acceptors have very similar absorption characteristics (not shown). The methyl and phenyl substitutions on the quinoline and phenoxazine moieties do not appear to affect the ground-state electronic structure of the phenoxazine-quinoline D−A molecules. For each D−A molecule, weak solvatochromism was observed in the ICT absorption band. For example, the ICT absorption maximum of PQx-PPO red-shifted from 472 nm in nonpolar triethylamine to 480 nm in moderately polar chloroform and then blue-shifted

(28) (a) Grabowski, Z. R.; Rotkiewicz, K.; Rettig, W. *Chem. Rev.* **2003**, *103*, 3899. (b) Bhattacharyya, K.; Chowdhury, M. *Chem. Rev.* **1993**, *93*, 507.

Table 1. Absorption Properties of D−A Molecules in Solvents of Varying Polarity[a]

solvent	BP-HPO	PQ-PPO	PQx-PPO	BQx-PPO	BzQx-PPO
triethylamine	390	420	431	472	462
toluene	398	426	439	475	468
chloroform	398	428	441	480	476
1,2-dichloroethane	400	429	438	478	468
acetonitrile	396	426	428	463	460

[a] Maximum of lowest-energy absorption band in each solvent (in nm).

to 463 nm in highly polar acetonitrile. The optical absorption properties of five D−A molecules in solvents of varying polarity are summarized in Table 1.

Figure 1b shows the normalized photoluminescence (PL) emission spectra of the five D−A molecules in dilute (2×10^{-5} M) dichloroethane solution. The emission spectra dramatically red shift with increasing electron-accepting strength. BP-HPO emits blue color in dichloroethane solution with a maximum at 463 nm and a full width at half-maximum (fwhm) of 63 nm. PQ-PPO has a green emission with PL maxima at 508 nm (fwhm = 82 nm). PQx-PPO with quinoxaline acceptor emits orange color in solution (PL max = 594 nm, fwhm = 110 nm). Red emission is observed from both BzQx-PPO and BQx-PPO with similar PL maxima (~645 nm) and fwhm (~120 nm). The reason for the observed red-shift with increasing electron acceptor strength is the greater degree of ICT (increasing excited-state dipole moments) in going from quinoline to quinoxaline to benzoquinoxaline or benzoylquinoxaline.[29] Thus, emission colors spanning the entire visible region are obtained from the phenoxazine-based D−A molecules, demonstrating how charge transfer and the resultant ICT fluorescence in a D−A molecule can be effectively manipulated through the electron-accepting strength of the acceptor building block. Table 2 summarizes the emission properties of the five D−A molecules.

Panels a and b in Figure 2 show the normalized PL emission spectra of BP-HPO and PQx-PPO, respectively, in solvents of varying polarity. Large positive solvatochromic effects were observed in the PL emission spectra, much larger than those in the absorption spectra, indicating stronger excited-state ICT character and larger dipole moments compared to the ground state. Both the emission maximum (λ_{max}^{PL}) and the fwhm increased dramatically with solvent polarity (Table 2). In the case of PQx-PPO, they varied from $\lambda_{max}^{PL} = 490$ nm (fwhm = 57 nm) in nonpolar triethylamine to 625 nm (fwhm = 130 nm) in highly polar acetonitrile. Similar large ICT effects were observed in the PL emission of other D−A molecules (Table 2). In the case of BQx-PPO and BzQx-PPO, the ICT emission was completely quenched in the highly polar environment of acetonitrile. In any given solvent, the Stokes shift increases in going from BP-HPO to PQ-PPO to BQx-PPO, again indicative of larger ICT effects with increasing electron acceptor strength. Thus, we anticipate that the excited-state dipole moment increases progressively in going from BP-HPO to PQ-PPO to BQx-PPO.

(29) Dini, D.; Yang, G. Y.; Hanack, M. *J. Chem. Phys.* **2003**, *119*, 4857.

The excited-state dipole moments of some of the molecules were estimated from the observed solvatochromism in PL emission using the Lippert−Mataga relationship.[30] Ground-state dipole moments ($\vec{\mu}_g$) of 0.72, 3.24, 3.26, and 2.21 D for PQ-PPO, PQx-PPO, BQx-PPO, and BzQx-PPO, respectively, were calculated using quantum-chemical methods.[26] The corresponding radii of the Onsager cavity (a_0) were calculated to be 6.67, 6.74, 6.93, and 7.42 Å, respectively, from their optimized ground-state geometries (see Table 3).[26] On the basis of these data, excited-state dipole moments ($\vec{\mu}_e$) of 17.11, 23.4, 23.53, and 25.5 D for PQ-PPO, PQx-PPO, BQx-PPO, and BzQx-PPO, respectively, were obtained. The much larger excited-state dipole moment relative to the ground-state in all molecules is clearly indicative of a greater ICT character in the excited state. As expected, the dipole moment of the excited-state increases steadily with increasing electron acceptor strength in the D−A molecule, due to greater charge separation in the excited state. This explains the observed trend in red-shift in the PL emission spectra (Table 2) of the molecules in going from PQ-PPO to PQx-PPO to BzQx-PPO.

Additional evidence supporting the stronger ICT interaction with increasing strength of the electron acceptor in the D−A molecules comes from their PL quantum yields (ϕ_f) in toluene solution. It is well-known that the ϕ_f value of a D−A molecule decreases with increasing excited-state ICT character.[11a,28] We found that the ϕ_f values of the D−A molecules decreased with increasing strength of the acceptor block (Table 4). High ϕ_f values of 0.86 and 0.74−0.81 were obtained for BP-HPO and the four phenoxazine-quinoline molecules. The ϕ_f values decreased to 0.52 in PQx-PPO to 0.41 in BzQx-PPO and to as low as 0.16 in BQx-PPO. This decreasing trend in PL quantum yield values in going from BP-HPO to BQx-PPO correlates very well with the estimated increasing excited-state dipole moments.

To further investigate the dynamics of the ICT emission, we measured the PL decay lifetimes of the emission maxima of the eight D−A molecules in dilute toluene solution. All the PL decay characteristics are collected in Table 4. The PL decays of all the molecules were well-described by single-exponential fits, suggesting emission from the intramolecular charge-transfer exciton. Figure 3 shows the PL decay curves for five representative D−A molecules. The lifetimes increased with increasing electron acceptor strength in the molecule, except for BQx-PPO. BP-HPO had a relatively short lifetime of 2.19 ns, whereas PQx-PPO and BzQx-PPO had longer lifetimes of 4 and 5 ns, respectively. Based on the measured ϕ_f in solution and the fluorescence lifetime (τ), we then estimated the

(30) The excited state dipole moments were calculated using the relation

$$\bar{\nu}_{flu} = \bar{\nu}_{flu}^{0} - \frac{1}{4\pi\varepsilon_0 hc}\frac{2}{a_0^3}\vec{\mu}_e(\vec{\mu}_e - \vec{\mu}_g)f(\varepsilon, n)$$

where

$$f(\varepsilon, n) = \frac{\varepsilon - 1}{2\varepsilon + 1} - \frac{1}{2}\left(\frac{n^2 - 1}{2n^2 + 1}\right)$$

= solvent polarity parameter ν_{flu} is the charge transfer emission maximum (cm^{-1}), ν_{flu}^{0} is the charge transfer emission maximum (cm^{-1}) extrapolated to the gas phase, a_0 is the radius of the Onsager cavity (nm), $\vec{\mu}_g$ and $\vec{\mu}_e$ are the ground- and excited-state dipole moments (D), respectively, ε is the dielectric constant of the solvent, and n is the refractive index of the solvent. For further details, see ref 28a.

Table 2. PL Emission Properties of D−A Molecules in Solvents of Varying Polarity[a]

	BP-HPO		PQ-PPO		PQx-PPO		BQx-PPO		BzQx-PPO	
solvent	λ^{PL} (nm)	fwhm (nm)	λ^{PL} (nm)	fwhm (nm)	λ^{PL} (nm)	fwhm (nm)	λ^{PL} (nm)	fwhm (nm)	λ^{PL} (nm)	fwhm (nm)
triethylamine	438	45	461	44	490	57	538	85	540	80
toluene	448	48	474	47	514	71	560	85	564	80
chloroform	455	54	492	66	572	100	620	102	622	100
1,2-dichloroethane	463	63	508	82	594	110	645	120	648	122
acetonitrile	475	75	530	102	625	130				

[a] Emission maximum and full width at half-maximum in each solvent are listed. No emission was detected for BQx-PPO and BzQx-PPO in acetonitrile.

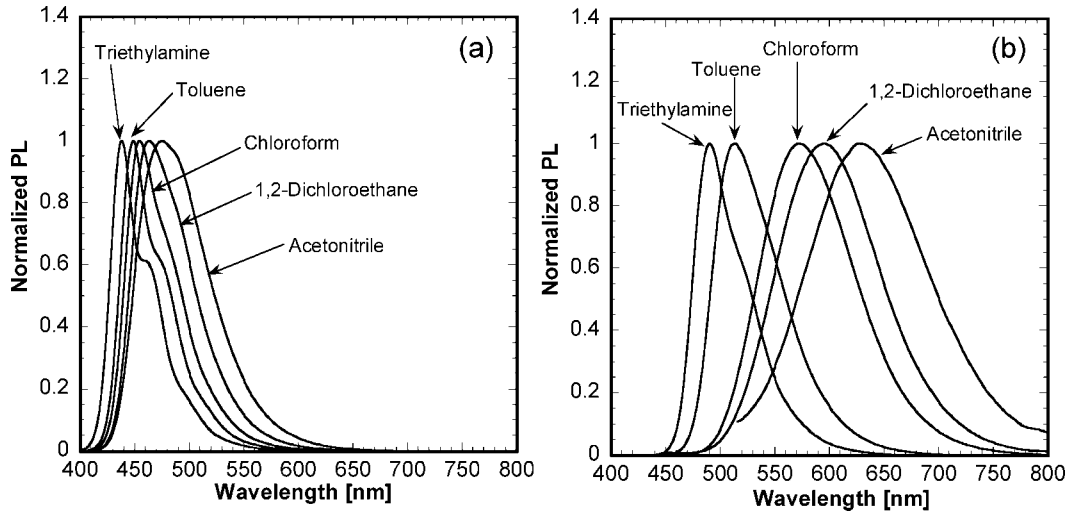

Figure 2. PL emission spectra of (a) BP-HPO and (b) PQx-PPO in solvents of varying polarity. Excitation wavelength is 400 nm for BP-HPO and 440 nm for PQx-PPO.

Table 3. Ground- and Excited-State Dipole Moments of D−A Molecules

	PQ-PPO	PQx-PPO	BQx-PPO	BzQx-PPO
radius of Onsager cavity (a_0, Å)[a]	6.67	6.74	6.93	7.42
ground-state dipole moment ($\vec{\mu}_g$, D)[a]	0.72	3.24	3.26	2.21
excited-state dipole moment ($\vec{\mu}_e$, D)[b]	17.11	23.40	23.53	25.50

[a] Estimated from quantum chemical calculations. [b] Estimated from solvatochromic data using the Lippert−Mataga relation. See ref 30.

radiative lifetime (τ_0) of the emission band according to $\phi_f = \tau/\tau_0$ and the rate constants for radiative (k_r) and nonradiative (k_{nr}) decay according to $\tau_0 = 1/k_r$ and $\tau = 1/(k_r + k_{nr})$. τ_0 values increased from 2.55 ns in BP-HPO to 7.71 ns in PQx-PPO to 12.2 ns in BzQx-PPO and finally to 16.0 ns in BQx-PPO. The four phenoxazine-quinoline molecules had similar τ_0 values of ~3.2−3.8 ns. BP-HPO had the largest radiative rate constant $k_r = 39 \times 10^7\ s^{-1}$ and smallest $k_{nr} = 6.7 \times 10^7\ s^{-1}$. BQx-PPO had $k_r = 6.3 \times 10^7\ s^{-1}$ and $k_{nr} = 32.8 \times 10^7\ s^{-1}$. The estimated k_r and k_{nr} values explain the observed trend in the PL quantum yield values of the D−A molecules. The efficiency of the ICT emission clearly decreases in going from BP-HPO to BQx-PPO. Overall, a factor of 5 reduction in PL efficiency is observed upon going from quinoline (PQ-PPO) to benzoquinoxaline (BQx-PPO) acceptor. Thus, although one can effectively tune the emission colors in a D−A molecule from blue to green to red by increasing the electron acceptor strength, it invariably comes at the expense of reduced charge-transfer fluorescence efficiencies in the red region, which could affect the ultimate OLED performance.

(b) Thin Films. The normalized optical absorption and PL emission spectra of thin films of five D−A molecules are shown in panels a and b in Figure 4, respectively. The solid-state absorption spectra are similar to those observed in dilute solution (Figure 1a). As in solution, two prominent features were observed: a broad lowest-energy structureless band and several structured high-energy bands below 340 nm. For example, BQx-PPO had its lowest-energy absorption maximum at 490 nm and three well-resolved vibronic peaks at 230, 280, and 310 nm. The lowest energy absorption band is of charge transfer character while the high-energy band is likely related to the rigid benzoquinoxaline moiety. As in solution, the thin film spectra red-shift steadily with increasing electron acceptor strength. BP-HPO had the highest optical absorption edge band gap of 2.64 eV while BQx-PPO and BzQx-PPO had the lowest band gaps of 2.14 eV. Thus, the band gap of the D−A molecules was tuned over a range of 0.5 eV by changing the electron accepting moiety in the molecule. All the four quinoline-based molecules had very similar absorption characteristics with comparable band gaps of 2.4−2.5 eV. The thin-film photophysical properties of the molecules are collected in Table 5.

The thin film PL emission spectra of the molecules, shown in Figure 4b, are similar to their dilute solution spectra in terms of line shape and fwhm. The emission maximum red-shifted from 473 nm in BP-HPO to 547 nm in PQx-PPO to 618 nm in BQx-PPO with increasing electron acceptor strength. Thus, the emission colors varied from blue (BP-

Table 4. PL Decay Characteristics of the D-A Molecules in 10^{-5} M Toluene Solutions[a]

molecule	monitored emission (nm)	τ (ns)	χ^2	φ_f	τ_0 (ns)	k_r ($\times 10^7$ s^{-1})	k_{nr} ($\times 10^7$ s^{-1})
BP-HPO	448	2.19	1.27	0.86	2.55	39.0	6.7
PQ-PPO	473	2.56	1.23	0.81	3.16	32.0	7.1
PQ-MPO	487	2.81	1.29	0.74	3.80	26.3	9.3
MQ-PPO	477	2.57	1.04	0.77	3.34	30.0	8.9
MQ-MPO	477	2.47	1.35	0.77	3.20	31.2	9.2
PQx-PPO	514	4.01	1.19	0.52	7.71	13.0	11.9
BQx-PPO	565	2.56	1.12	0.16	16.0	6.3	32.8
BzQx-PPO	560	5.00	1.11	0.41	12.2	8.2	11.8

[a] Excitation wavelength = 381 nm. Fits to all the PL decays were single exponential.

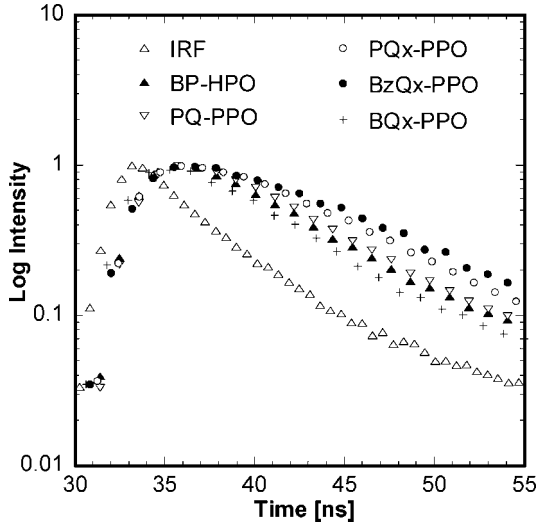

Figure 3. Fluorescence decay curves of the PL emission peak of the donor−acceptor molecules in 1×10^{-5} M toluene solutions with 381 nm excitation. IRF denotes the instrument response function.

HPO) to green (PQ-PPO) to yellow (PQx-PPO) and red (BQx-PPO and BzQx-PPO) as indicated by the CIE emission coordinates in Table 5. In addition to the observed red-shift, the fwhm of the emission spectra increased from 54 nm in BP-HPO to 75 nm in PQx-PPO to 84 nm in BQx-PPO with increase in electron acceptor strength. This can partly be explained by the increasing charge transfer character of the excited-state in going from BP-HPO to BQx-PPO, as previously discussed in dilute solution. These PL emission bands of the thin films of the molecules originate from their ICT excited states as evidenced by previously discussed strong positive solvatochromism in solution (Table 2). Although the solid-state PL quantum yields were not measured, it was clear from the measured fluorescence intensity of thin films of comparable thicknesses that the fluorescence efficiency decreased with increasing electron acceptor strength, as in solution (Table 4), i.e., BP-HPO films were the most fluorescent and BQx-PPO films were the least emissive among the eight molecules. Both BQx-PPO and BzQx-PPO had identical, nearly overlapping, thin film emission spectra; however, it was clear that BzQx-PPO thin films had a much higher ϕ_f value than BQx-PPO thin films.

Among the four quinoline-containing molecules, the PL emission maxima varied from 500 nm in MQ-MPO to 539 nm in PQ-MPO. Thus, although MQ-MPO films had pure green emission, the PQ-MPO thin films emitted greenish-yellow colors. A similar extent of ICT character is expected in the four molecules because of the common quinoline acceptor moiety. The observed differences in the emission characteristics among the four phenoxazine-quinoline molecules are likely related to the subtle variations in the thin film morphology due to varying degrees of intermolecular stacking interactions caused by the methyl and phenyl groups. MQ-MPO films seemed to crystallize partially over time, whereas the other films stayed optically clear over the same lengths of time. The presence of methyl groups both on the phenoxazine and quinoline moieties apparently enhances the $\pi-\pi$ stacking interactions, which are known to reduce the solid-state fluorescence efficiencies,[13b] whereas the bulkier phenyl groups preclude such interactions. Thus, on visual inspection, PQ-PPO films were the most fluorescent, MQ-MPO films were the least fluorescent and the PQ-MPO and MQ-PPO films had intermediate fluorescence efficiencies. These results have a significant bearing on the electroluminescent properties of these four D−A molecules as discussed later. Overall, the solid-state emission colors were tuned over the entire visible region by changing the strength of the electron accepting moiety in the D−A molecule, while keeping the same central donor block.

Electroluminescence Properties. All OLED fabrication and characterization steps were performed under ambient laboratory air with no device encapsulation. Diodes of the type ITO/PEDOT/PVK (10 nm)/D-A molecule (35 nm)/TPBI (30 nm)/LiF (2 nm)/Al were fabricated with all the D−A molecules. Figure 5a−e shows the normalized EL emission spectra of such diodes based on five of the eight D−A molecules. In each diode, the EL emission is very similar to the thin film PL emission of the D−A molecule and can be attributed to its ICT excited state formed by the recombination of the phenoxazine radical cation with the radical anion of the acceptor moiety. For example, the EL emission maxima of the PQ-PPO diodes (Figure 5b) ranged from 505−515 nm over the entire operating voltage range which is similar to its thin film PL emission maximum (Table 5). Stable yellow emission was obtained from the PQx-PPO diodes (Figure 5c) with CIE coordinates of (0.41, 0.57) that did not change much over the entire drive voltage. Blue emission was obtained from the BP-HPO diodes (Figure 5a), whereas diodes based on BQx-PPO and BzQx-PPO emitted red color (panels d and e in Figure 5). Thus, the EL emission colors spanned the entire visible region as shown in the CIE plot in Figure 5f. A summary of the EL emission coordinates from all the molecules is presented in Table 6.

Panels a and b in Figure 6 show the current density−voltage and luminance−voltage plots of four diodes based on PQ-PPO, PQx-PPO, BQx-PPO, and BzQx-PPO. All the diodes had an identical low turn-on voltage of 4 V. The maximum

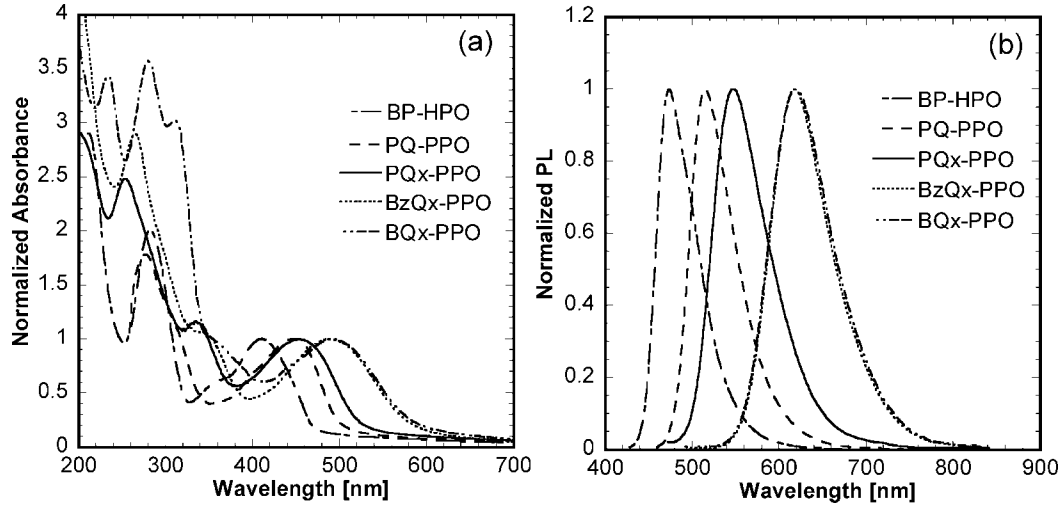

Figure 4. (a) Normalized optical absorption spectra and (b) PL emission spectra of thin films of five donor−acceptor molecules.

Table 5. Absorption and Emission Properties of the D−A Molecules in Thin Films

molecule	λ_{max}^{abs} (nm)	E_g^{opt} (eV)[a]	E_g^{el} (eV)[b]	λ_{max}^{PL} (nm)[c]	fwhm (nm)[d]	CIE (x, y)
BP-HPO	410	2.64		473	54	(0.14, 0.26)
PQ-PPO	447	2.48	2.8	515	60	(0.26, 0.63)
PQ-MPO	450	2.40	2.7	539	71	(0.36, 0.60)
MQ-PPO	435	2.53	2.8	507	60	(0.25, 0.59)
MQ-MPO	450	2.43	2.8	500	64	(0.28, 0.55)
PQx-PPO	453	2.36	2.5	547	75	(0.40, 0.58)
BQx-PPO	490	2.14	2.2	618	84	(0.63, 0.37)
BzQx-PPO	490	2.14	2.2	618	80	(0.63, 0.37)

[a] Optical band gap derived from the absorption onset of the thin film spectrum. [b] Electrochemical band gap values taken from ref 26. [c] The thin films were excited at their absorption maximum. [d] Full width at half-maximum of thin film PL emission spectrum.

brightness of the diodes varied from 1750 cd/m^2 in BQx-PPO diodes to as high as 36190 cd/m^2 in the PQ-PPO diodes. Devices from BzQx-PPO and PQx-PPO had intermediate brightnesses of 9580 and 25300 cd/m^2, respectively. The best performance among all the molecules was given by PQ-PPO with a maximum brightness of 36190 cd/m^2 at 10.7 V (Table 6). The maximum external quantum efficiency (EQE) of the device was 3.29% at a brightness of 5115 cd/m^2 with a luminous efficiency of 10.93 cd/A and power efficiency of 4.46 lm/W. The maximum EQE of the red-emitting BzQx-PPO diode was 1.44% at a brightness of 233 cd/m^2, which is fairly high for a nondoped fluorescent red emitter.[6d,e,12a,b] The observed trends in device performance correlated very well with the PL quantum yield of the D−A molecules, except for BP-HPO. PQ-PPO gave the best performance while BQx-PPO with the lowest PL quantum yield gave the poorest performance. We note that diodes based on BP-HPO gave poor and inconsistent performance with a maximum brightness of <100 cd/m^2; this diode also had very low current densities (<20 mA/cm^2). The plausible reasons for the poor performance are discussed later. Among the four quinoline-based molecules, the maximum brightness varied from 9670 cd/m^2 in MQ-MPO diodes to 36190 cd/m^2 in PQ-PPO, whereas PQ-MPO and MQ-PPO had intermediate luminances. Thus, among the four molecules, MQ-MPO gave the lowest performance as indicated by the brightness and efficiency values in Table 6.

Figure 7a shows the luminous efficiencies as a function of the current density of the diodes for PQ-PPO, PQx-PPO, BQx-PPO, and BzQx-PPO. Among these four molecules, the superior performance of the PQ-PPO diodes is evident. The luminous efficiency of the diodes remains fairly constant over a wide range of current densities. It decreases from a maximum of 10.93 cd/A (at 47 mA/cm^2) to 7.24 cd/A at the highest current densities (500 mA/cm^2) in the PQ-PPO diodes. In the PQx-PPO devices, it varies from a maximum of 8 cd/A (at 91 mA/cm^2) to 5.58 cd/A at 452 mA/cm^2. The lowest efficiencies were obtained in the BQx-PPO diodes in the range of 0.35−0.43 cd/A. Thus, the maximum efficiency of the PQ-PPO diodes is ∼25 times higher than that of the BQx-PPO devices. Figure 7b shows the variation in the luminous efficiencies with the brightness of the diodes based on the four phenoxazine-quinoline D−A molecules. Although the donor and acceptor moieties in all four molecules are identical, significant differences in the device performance are observed among the four molecules, highlighting the importance of the methyl and phenyl substitutions on the D/A moieties. Clearly, PQ-PPO had the best performance (maximum brightness and efficiency), whereas MQ-MPO had the lowest performance among the four molecules. MQ-PPO had the second best performance as the emissive layer, whereas PQ-MPO was third best. The maximum brightness and efficiency in the PQ-PPO diodes were higher by factors of 3.7 and 3.1, respectively, compared to those in the MQ-MPO diodes.

To understand the observed variation in the device performance among the eight D−A molecules, we now discuss the energy level diagram of the diodes as shown in Figure 8. The energy levels of the phenoxazine D−A molecules were estimated from cyclic voltammetry measure-

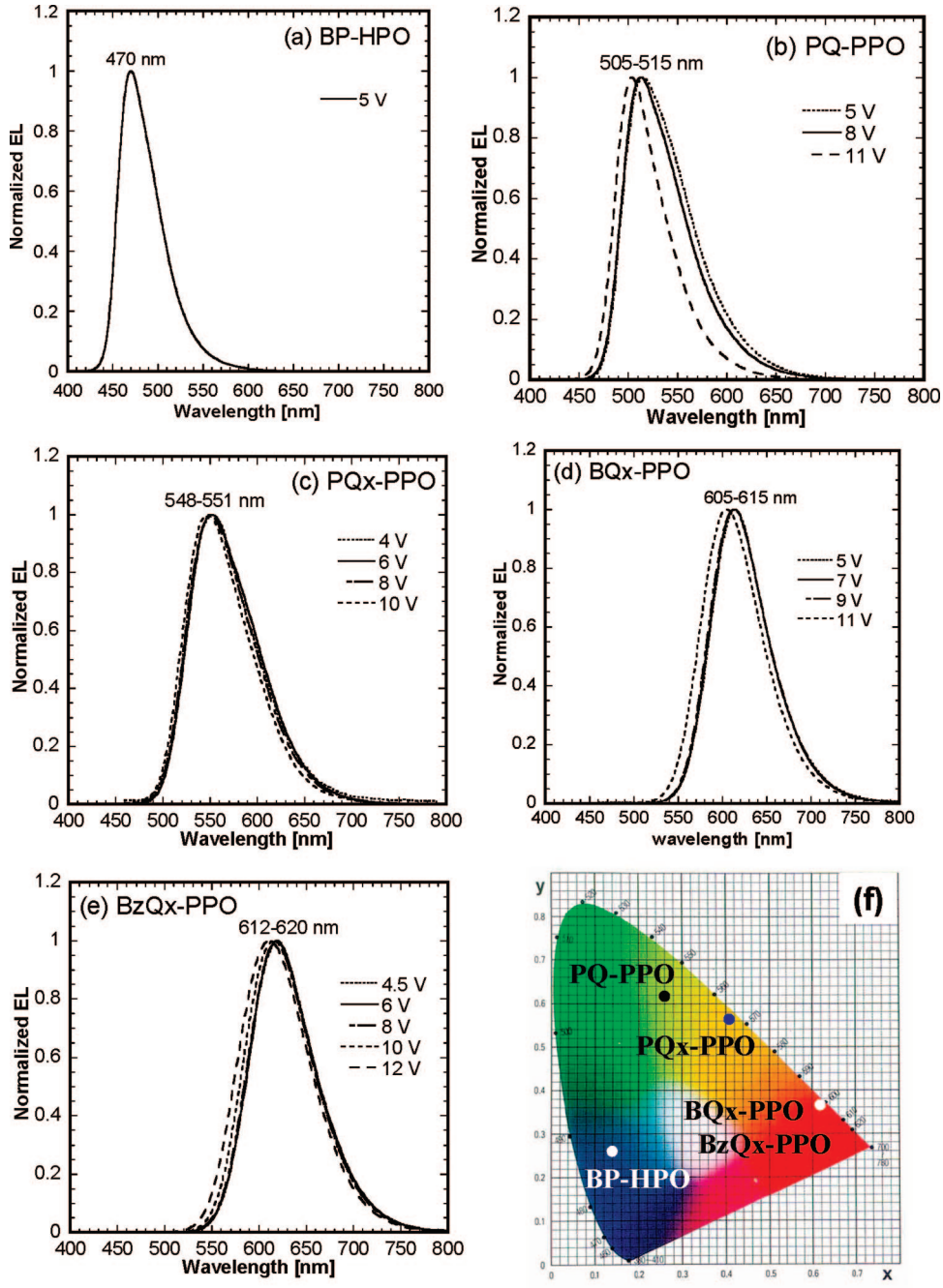

Figure 5. EL spectra of ITO/PEDOT/PVK/D-A molecule/TPBI/LiF/Al OLEDs: (a) BP-HPO, (b) PQ-PPO, (c) PQx-PPO, (d) BQx-PPO, and (e) BzQx-PPO. (f) A plot of the CIE coordinates of OLEDs from the D−A molecules.

Table 6. Device Characteristics of OLEDs from D−A Molecules: ITO/PEDOT/PVK (10 nm)/D−A Molecule (35 nm)/TPBI (30 nm)/LiF/Al[a]

molecule	V_{on} (V)[b]	drive voltage (V)	J (mA/ cm^2)[c]	L (cd/m^2)[d]	device efficiency (cd/A, lm/W, %EQE[e])	λ_{max}^{EL}; fwhm (nm)[f]	CIE 1931 (x, y)
PQ-PPO	4.0	10.7 *7.7*	500 *47*	36190 *5115*	7.24, 2.11, 2.48 *10.93*, *4.46*, *3.29*	505; 58 *513*; *70*	(0.20, 0.58) (*0.27*, *0.61*)
PQ-MPO	4.0	10.9 *9.3*	500 *111*	12535 *4120*	2.50, 0.72, 0.69 *3.70*, *1.25*, *1.02*	529; 69 *529*; *69*	(0.33, 0.62) (*0.33*, *0.62*)
MQ-PPO	4.0	9.6 *8.3*	500 *160*	23020 *9495*	4.60, 1.50, 1.67 *5.91*, *2.22*, *2.15*	500; 58 *500*; *58*	(0.21, 0.55) (*0.21*, *0.55*)
MQ-MPO	4.0	11.6 *9.0*	500 *44*	9670 *1535*	1.93, 0.52, 0.56 *3.46*, *1.20*, *1.01*	525; 70 *527*; *77*	(0.33, 0.61) (*0.34*, *0.60*)
PQx-PPO	4.0	10.5 *8.1*	452 *91*	25300 *7280*	5.58, 1.68, 1.50 *8.00*, *3.10*, *2.20*	548; 80 *551*; *80*	(0.40, 0.58) (*0.41*, *0.57*)
BQx-PPO	5.0	12.5 *9.7*	500 *48*	1750 *210*	0.35, 0.09, 0.20 *0.43*, *0.14*, *0.24*	605; 79 *613*; *77*	(0.59, 0.41) (*0.62*, *0.38*)
BzQx-PPO	4.0	12.1 *7.9*	500 *10*	9580 *233*	1.92, 0.50, 1.19 *2.30*, *0.92*, *1.44*	612; 87 *618*; *80*	(0.60, 0.40) (*0.63*, *0.37*)

[a] Values in italic correspond to those for maximum device efficiencies at a practical brightness of ≥100 cd/m^2. [b] Turn-on voltage (at which EL is visible to the eyes). [c] Current density. [d] Luminance. [e] EQE = External quantum efficiency. [f] Emission maximum and full width at half-maximum of EL emission spectra.

ments reported in part 1.[26] Let us first consider the four phenylphenoxazine D−A molecules containing four different acceptors including quinoline, quinoxaline, benzoylquinoxaline and benzoquinoxaline (Figure 7a). The efficiency of an OLED depends both on the balance of electrons and holes and the solid-state PL quantum yield of the emitter.[1b] The

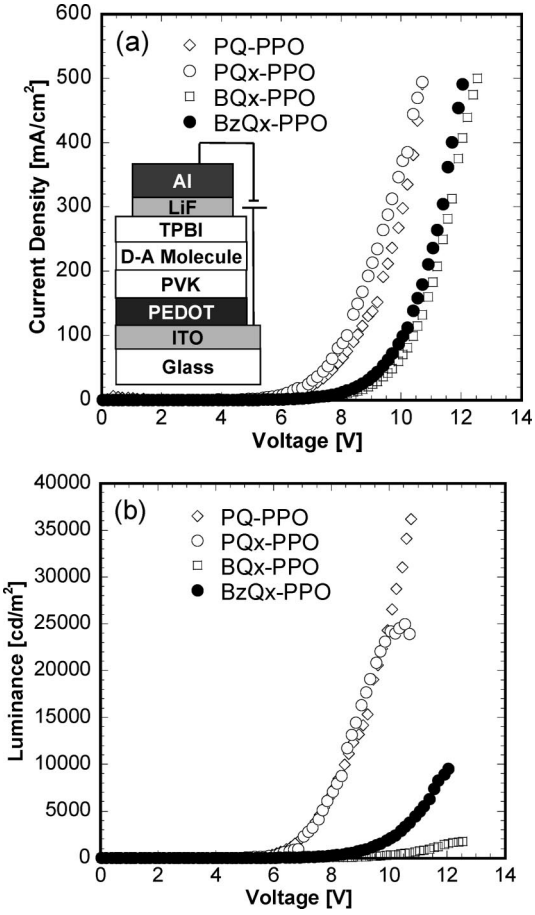

Figure 6. (a) Current density−voltage characteristics of diodes from four donor−acceptor molecules. The inset shows the device schematic. (b) Luminance−voltage characteristics of the devices in (a).

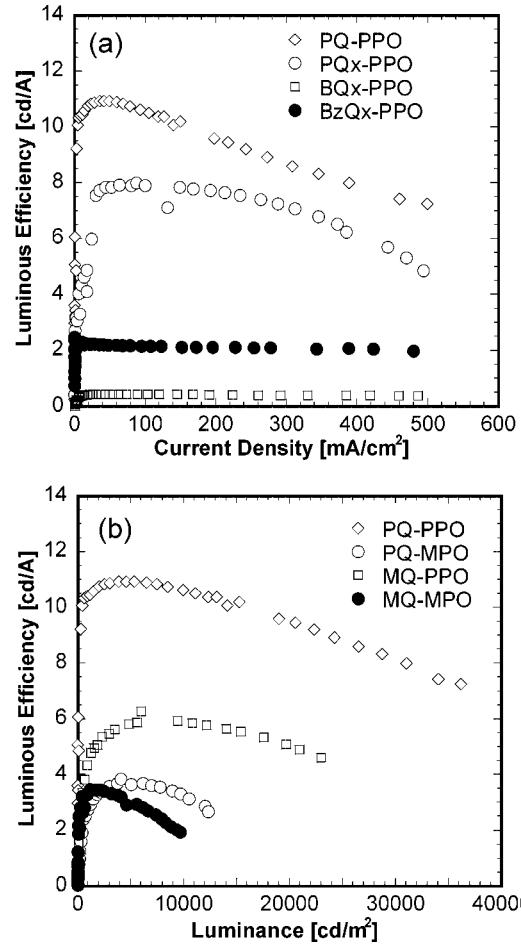

Figure 7. (a) Variation in luminous efficiency with the current density of the diodes of the four D−A molecules shown in Figure 6. (b) Luminous efficiency as a function of the luminance of the diodes based on the four phenoxazine-quinoline D−A molecules.

IP values of the four molecules are nearly identical at 5.1−5.2 eV,[26] suggesting similar hole injection and transport characteristics. The EA of the molecule increases from 2.4 eV in PQ-PPO to 2.7 eV in PQx-PPO to 3.0 eV in BQx-PPO and BzQx-PPO.[26] Electron injection from the TPBI layer into the D−A molecule layer should become relatively easier with increasing EA of the D−A molecule. Thus, electron injection into BQx-PPO should be easier than that into PQ-PPO, presumably leading to better charge recombination efficiency in the former. However, the PL quantum efficiency of the D−A molecule ultimately determines the device performance. The trend in device luminous efficiencies in Figure 7a matches very well with the observed decrease in PL quantum efficiencies in going from PQ-PPO to PQx-PPO to BzQx-PPO to BQx-PPO (Table 4) due to increasing excited-state ICT character with increasing electron acceptor strength. Hence, although BQx-PPO may have better electron injection/transport characteristics than PQ-PPO, the factor of 5 lower PL quantum efficiency of the former leads to inferior device performance in the BQx-PPO diodes. The observed unexpected poor performance of the BP-HPO diodes cannot simply be explained using the PL quantum yield argument because the BP-HPO films were very fluorescent. BP-HPO had a reversible electrochemical oxidation and a low IP of 5.0 eV,[26] suggesting good hole transport. However, no electrochemical reduction wave was

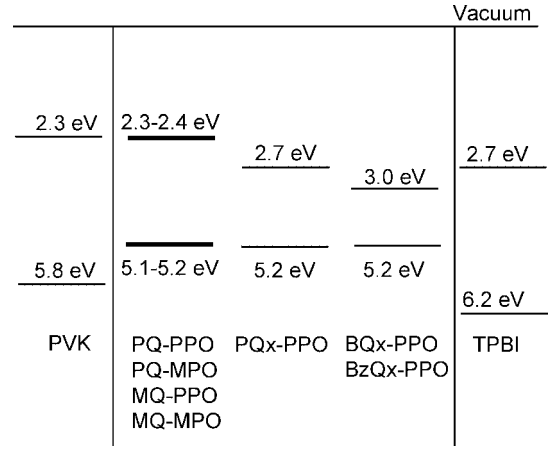

Figure 8. Energy levels (EA/ IP) of all the emissive D−A molecules and hole/electron-blocking materials (PVK, TPBI) used in the OLEDs.

detected, which can be explained by the fact that the biphenyl moiety is a very weak electron acceptor. This suggests very poor electron injection and transport characteristics in BP-HPO diodes. We believe that it is this lack of electron transporting ability that leads to the observed poor OLED performance from BP-HPO, despite its high fluorescence efficiency.

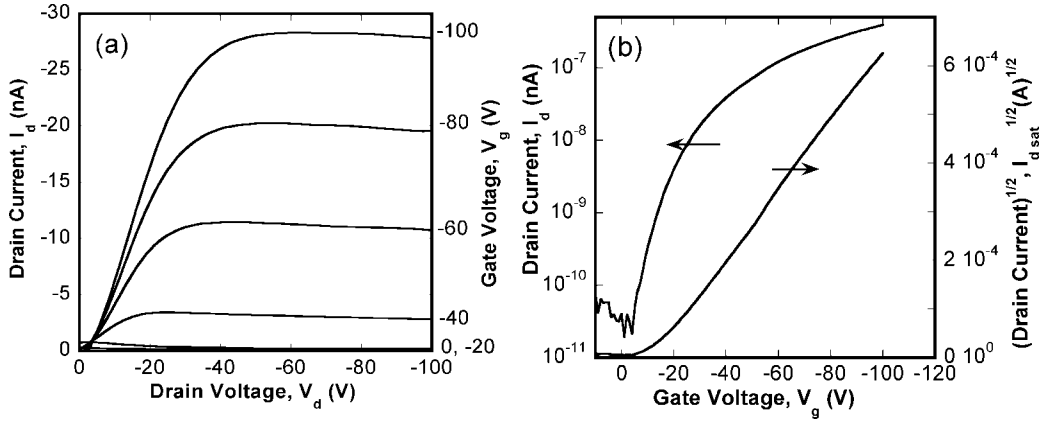

Figure 9. (a) Output characteristics and (b) transfer characteristic of a MQ-PPO FET.

We now discuss the significant differences in device performance from the four phenoxazine-quinoline D−A molecules (Figure 7b). The similar electrochemical properties with identical EA and IP values among these four molecules imply very similar charge (hole and electron) injection characteristics.[26] The charge transport characteristics may differ slightly due to differences in thin film morphologies. However, the device efficiency will largely be determined by the PL quantum yield of the four D−A molecules. In solution, all four molecules had similar PL quantum yields (Table 4), suggesting comparable excited-state ICT character. In thin films relevant to OLED performance, the fluorescence intensity decreased in the order PQ-PPO > MQ-PPO > PQ-MPO > MQ-MPO, as discussed previously in the thin film photophysics. Given the propensity of quinoline-based molecules to form excimers in the solid state,[3,13b,24b,c] we believe that the methyl groups on both quinoline and phenoxazine moieties lead to enhanced $\pi-\pi$ stacking interactions thereby quenching the fluorescence in the solid state. The inferior EL performance of MQ-MPO among the four molecules is thus a direct consequence of its lower solid-state PL quantum yield due to relatively stronger intermolecular interactions in thin films. Thus, although the electronic energy levels of the four D−A molecules are identical, the variations in the thin-film morphology due to differences in molecular structure may lead to the significantly varying EL efficiencies among them.

Thin Film Transistors. Field-effect transistors (FETs) based on thin films of the four phenoxazine-quinoline D−A molecules showed p-channel behavior with excellent saturation characteristics. Panels a and b in Figure 9 show respectively the output and transfer characteristics of a MQ-PPO FET. The hole mobility calculated using the saturation region transistor equation for the MQ-PPO FET is 7×10^{-4} cm^2/Vs. Similarly measured saturation region hole mobility for PQ-PPO, PQ-MPO, and MQ-MPO was 3×10^{-5}, 8×10^{-5}, and 1×10^{-6} cm^2/Vs, respectively. These hole mobilities in the phenoxazine-based D−A molecules are comparable to those previously reported in phenoxazine-based conjugated polymers.[21a] The observation of field-effect hole transport in thin films deposited onto substrates at room temperature clearly suggests that the rigid phenoxazine moiety is a useful building block for developing p-type semiconductors with low ionization potential (∼5.1 eV). n-Channel behavior was not observed in any of the four molecules, which could be partly explained by the large electron injection barriers of ∼2.7 eV from gold ($\Phi = 5.1$ eV) into the LUMOs of the molecules. Although the field-effect carrier mobility is not high, the low ionization potentials, the ambipolar redox properties, and the high solid-state fluorescence and electroluminescence efficiencies of the phenoxazine-based D−A molecules make them attractive candidates for applications in organic light-emitting transistors.[31]

Conclusions

We have investigated the photophysical, field-effect charge transport, and electroluminescent properties of a series of 8 new emissive donor−acceptor materials based on phenoxazine donor and different electron acceptors including quinoline, quinoxaline, benzoquinoxaline and benzoylquinoxaline. With increasing strength of the electron acceptor in the D−A molecule, the intramolecular charge transfer emission colors progressively red-shifted from blue to red. Strong positive solvatochromism was observed in the solution photoluminescence of the D−A molecules. The optical band gaps of the molecules varied from 2.64 eV in the phenoxazine-biphenyl molecule to as low as 2.14 eV in the phenoxazine-benzoquinoxaline molecule owing to the increasing charge-transfer character of the absorption. The thin-film emission colors spanned the visible, from greenish-blue (CIE = 0.14, 0.26) in BP-HPO to red (CIE = 0.63, 0.37) in BzQx-PPO. High-performance green OLEDs (36190 cd/m^2, 10.9 cd/A and 3.3% external quantum efficiency at 5115 cd/m^2) were achieved from the phenylphenoxazine-phenylquinoline molecule (PQ-PPO). On the other hand, red OLEDs with moderate performance (9580 cd/m^2, 2.3 cd/A at 230 cd/m^2) were obtained from the phenoxazine-benzoylquinoxaline molecule (BzQx-PPO). The observed reduction in device performance with increasing electron-acceptor strength of the D−A molecules can be explained by the decreasing fluorescence quantum yield. These results clearly show that the electron-accepting strength of the

(31) Muccini, M. *Nat. Mater.* **2006**, *5*, 605.

acceptor moiety in a D−A molecule is a powerful tool to manipulate its HOMO/LUMO energy levels and the resultant fluorescence and electroluminescence colors. Field-effect hole mobilities of up to 7×10^{-4} cm^2/Vs were obtained in the phenoxazine-quinoline molecules, suggesting that phenoxazine is a useful building block for developing p-type semiconductors for organic electronics and in particular emissive and charge transport materials for OLEDs.

Acknowledgment. This research was supported by the NSF (CTS-0437912), the NSF MDITR (DMR-0120967) and the Air Force Office of Scientific Research EHSS MURI (Grant F9550-06-1-0326).

CM7022136